Selective Catalytic Reduction of NOx with NH3 on Cu-, Fe-, and Mn-Zeolites Prepared by Impregnation: Comparison of Activity and Hydrothermal Stability

Putluru, Siva Sankar Reddy; Schill, Leonhard; Jensen, Anker Degn; Fehrmann, Rasmus S. N.

Published in:
Journal of Chemistry

Link to article, DOI:
10.1155/2018/8614747

Publication date:
2018

Document Version
Publisher's PDF, also known as Version of record

Hindawi
Journal of Chemistry
Volume 2018, Article ID 8614747, 11 pages
https://doi.org/10.1155/2018/8614747

Research Article

Selective Catalytic Reduction of NO_x with NH_3 on Cu-, Fe-, and Mn-Zeolites Prepared by Impregnation: Comparison of Activity and Hydrothermal Stability

Siva Sankar Reddy Putluru,[1,2] Leonhard Schill,[1,2] Anker Degn Jensen,[2] and Rasmus S. N. Fehrmann[1]

[1]*Centre for Catalysis and Sustainable Chemistry, Department of Chemistry, Technical University of Denmark, Building 207, DK-2800 Kgs. Lyngby, Denmark*
[2]*CHEC Research Center, Department of Chemical and Biochemical Engineering, Technical University of Denmark, Building 229, DK-2880 Kgs. Lyngby, Denmark*

Correspondence should be addressed to Rasmus S. N. Fehrmann; rf@kemi.dtu.dk

Received 30 August 2018; Revised 16 October 2018; Accepted 18 November 2018; Published 10 December 2018

Academic Editor: Davut Avci

Cu-, Fe-, and Mn-zeolite (SSZ-13, ZSM-5, and BEA) catalysts have been prepared by incipient wetness impregnation and characterized by N_2 physisorption, H_2-TPR, NH_3-TPD, and XPS methods. Both metal and zeolite support influence the deNO_x activity and hydrothermal stability. Cu-zeolites and Mn-zeolites showed medium temperature activity, and Fe zeolites showed high temperature activity. Among all the catalysts, Cu-SSZ-13 and Fe-BEA are the most promising hydrothermally resistant catalysts. Fresh and hydrothermally treated catalysts were further examined to investigate the acidic and redox properties and the zeolite surface composition. Increased total acidity after metal impregnation and loss of acidity due to hydrothermal treatment were observed in all the catalysts. Hydrothermal treatment resulted in migration of metal or in strong metal support interations, whereby changes in reduction patterns are observed.

1. Introduction

The selective catalytic reduction (SCR) of nitrogen oxides (NO_x) with ammonia as the reducing agent is important for minimizing harmful emissions from combustion and high temperature processes [1–3]. The process is currently being used extensively to reduce the NO_x from stationary sources (especially power plants), and SCR technology has also obtained increasing attention for reduction of NO_x from diesel vehicle emissions [4].

The most widely used SCR catalyst for reduction of NO_x is vanadia supported on TiO_2 (anatase) promoted with WO_3 or MoO_3. However, $V_2O_5/WO_3(MoO_3)$-TiO_2 has some shortcomings regarding high activity for oxidation of SO_2 to SO_3, toxicity, and lack of high-temperature stability which highly limits its applicability in the automotive sector [4]. In addition, there is the problem of the transformation of the anatase to the rutile phase at high temperatures leading to catalyst deactivation. The first SCR systems were installed on power plants in the late 1970's and early 1980's. It was realized already at this time that metal-zeolite catalysts based upon a metal like copper possessed high activity for the decomposition of NO, even in the absence of a reducing agent [5]. More recently, especially the interest in automotive SCR has initiated a lot of research within the metal-zeolite systems [4, 6]. Initial studies have reported that lack of hydrothermal stability at high temperatures is one of the commercially limiting factors. However, recent development and demonstration of small pore Cu-SSZ-13 and Cu-SAPO-34 catalysts have received substantial attention due to their outstanding activity and hydrothermal stability [6–14]. Recent reports have shown that Cu-SAPO catalysts suffer

from poor hydrothermal stability at very low temperatures (70°C) caused by the breakage of the Si-O-Al bonds [15]. The hydrothermal stability at low temperatures can be somewhat increased by doping with Ce [16]. Furthermore, Cu-CHA has the advantage of generating N_2O only at low levels [6].

At low temperatures, metal-zeolite reaction mechanisms are considered to be Langmuir–Hinshelwood type [14, 17, 18]. Metal-zeolites contain metal ions which are very well dispersed to interact with NO to form NO_2 and zeolite acid sites to interact with NH_3 to form NH_4^+ ions. NO_2 and adjacent NH_4^+ ions further react to produce N_2 and H_2O [17–20]. It has been proposed that NO_2 is the reactive species for the SCR of NO_x with NH_3 on zeolite catalysts and that the oxidation of NO to NO_2 is the rate-limiting step [18]. The suggested mechanistic explanations for reactions over the promising Cu-CHA system at high temperatures are completely different from the Langmuir-Hinshelwood type ones used for the low temperature regime [8, 11]. Janssens et al. [14] proposed a catalytic cycle proceeding on a single Cu ion. The oxidation of NO to NO_2 is the rate-determining step, and there is no need for Brønsted acid site participation. The NO_2 then engages in a "fast SCR"-like step. Falsig et al. [13] have shown using density functional theory calculations that proximity to another Cu ion can decrease the activation energy of NO oxidation and is in good agreement with experimental studies [21].

In the present work, we report on the influence of Cu, Fe, and Mn metals supported on zeolite supports (SSZ-13, BEA, and ZSM-5) on the SCR activity and hydrothermal stability. The catalysts were characterized by means of nitrogen physisorption, NH_3-TPD, H_2-TPR, and XPS techniques. The characteristics were further related to the catalytic performance for SCR of NO with NH_3.

2. Experimental

2.1. Catalyst Preparation and Characterization. Pure ZSM-5 and BEA supports were obtained from Zeolyst International. SSZ-13 support was supplied by Haldor Topsøe A/S, and the synthesis was reported recently [22]. 3 wt.% Cu, 3 wt.% Fe, and 3 wt.% Mn-zeolite catalysts were prepared by incipient wetness impregnation using appropriate amounts of copper nitrate trihydrate, iron nitrate nonahydrate, and manganese acetate tetrahydrate (Aldrich, 99.9%) as precursors, respectively, and SSZ-13 (Si/Al = 13), ZSM-5 (Si/Al = 15), or BEA (Si/Al = 12.5) as supports. The prepared catalysts were oven-dried at 120°C for 12 h and finally calcined at 500°C for 5 h before use.

A portion of the catalysts was also treated under mild hydrothermal conditions at a total flow rate of 1100 mL/min of a gas containing 11 vol% H_2O in air at 650°C for 3 h.

BET surface areas of the samples were determined from nitrogen physisorption measurements on about 100 mg sample at liquid nitrogen temperature with a Micromeritics ASAP 2010 instrument. The samples were kept at 200°C for 1 h before the measurement.

NH_3-TPD (temperature-programmed desorption) experiments were performed on a Micromeritics Autochem-II instrument. In an usual experiment, 100 mg of the dehumidified sample was inserted into a quartz reactor and treated in a flow of 50 $cm^3 \cdot min^{-1}$ of He at 100°C for 1 h. Afterwards, the sample was treated with anhydrous NH_3 gas (Air Liquide, 5% NH_3 in He) for 2 h at 100°C. After ammonia adsorption, the sample was flushed with He (50 mL/min) for 100 min at 100°C. The NH_3 desorption operation was carried out by heating the sample from 100 to 700°C (10°C/min) under a flow of He (25 mL/min).

H_2-TPR (temperature-programmed reduction) measurements were performed on a Micromeritics Autochem-II instrument. 100 mg of the dried sample was placed in one arm of a U-shaped quartz tube on quartz wool. TPR analysis was performed under a flow of 50 mL/min of 4% H_2 and balance Ar (Air Liquide) from 50°C to 850°C with a ramp rate of 10°C/min. The hydrogen concentration was monitored using a thermal conductivity detector (TCD).

XPS (X-ray photoelectron spectroscopy) measurements were conducted on a Thermo scientific system at room temperature using Al K_{alpha} radiation (1484.6 eV). Before acquisition of the data, the sample was outgassed for about 1 h under vacuum to minimize surface contamination. The XPS instrument was calibrated using Au as the standard. To avoid surface charges caused by irradiation, a short exposure time is used to acquire the spectrum [23].

2.2. Catalytic Activity Measurements. The SCR activity measurements were carried out at atmospheric pressure in a fixed-bed quartz reactor loaded with about 10 mg of the catalyst (180–300 μm) positioned between two layers of quartz wool. The gas composition was 1000 ppm NO, 1100 ppm NH_3, 3.5% O_2, 2.3% H_2O, and N_2 (remaining). The total flow rate was 300 $cm^3 \cdot min^{-1}$ (ambient conditions). During the experiments, the temperature was raised in steps of 25°C from 200 to 600°C, while the NO and NH_3 concentrations were monitored by a Thermo Electron's Model 17C chemiluminescence NH_3-NO_x gas analyzer. N_2O concentration was measured by gas chromatography (Shimadzu-14B GC, TDC detection, Poraplot column). The activity was measured after reaching the steady state. Fresh and hydrothermally treated catalysts were compared by change in relative activity (%) of the corresponding catalysts.

Since the SCR reaction is known to be first-order with respect to NO under stoichiometric NH_3 conditions [24], the activity can be represented by the first-order rate constant k ($cm^3 \cdot g^{-1} \cdot s^{-1}$), which can be obtained from the conversion of NO by the following equation:

$$k = -\frac{F}{w} * \ln(1 - x) \quad (1)$$

where F denotes the flow rate (cm^3/s), w denotes the catalyst mass, and X denotes the fractional conversion of NO.

3. Results and Discussion

3.1. Catalyst Characterization

3.1.1. Support Properties. The results of surface area ($m^2 \cdot g^{-1}$), pore size (Å), Si/Al ratios, and acidity ($\mu mol \cdot g^{-1}$) of the zeolite supports are summarized in Table 1. The surface

Table 1: Physical characterization of support materials.

Support	Si/Al	Pore size (Å)[a]	Surface area ($m^2 \cdot g^{-1}$)	Total acidity (μmol $NH_3 \cdot g^{-1}$)
SSZ-13	13.1	3.8 × 3.8	655	1277
BEA	12.5	6.6 × 7.7	640	1008
ZSM-5	15	5.3 × 5.6	430	1062

[a]http://www.iza-structure.org/default.htm.

areas of the supports are decreasing in the order SSZ-13 (655) > BEA (640) > ZSM-5 (430). Based on the pore size of the supports, SSZ-13 (3.8 × 3.8 Å) is a small pore zeolite, ZSM-5 (5.3 × 5.6 Å) is a medium pore zeolite, and BEA (6.6 × 7.7 Å) is a large pore zeolite.

3.1.2. NH_3-TPD. Temperature-programmed desorption (TPD) of a basic molecule, especially ammonia, is a convenient method for quick determination of the acidic properties of a solid acid material [25, 26]. From NH_3-TPD, total acidity, strength, and distribution can be obtained from the peak area, position, and shape, respectively. Figure 1 shows NH_3-TPD profiles of the zeolite supports in the temperature range 100–700°C. Pure zeolite supports show two ammonia desorption regions: one due to weak acid strength and the other due to moderate acid strength. The weak acid sites were observed at lower temperatures, i.e., around 200°C, while the moderate acid sites were observed between 400 and 500°C [25]. The moderate acid strength of the zeolite supports is in the order SSZ-13 (473°C) > BEA (457°C) > ZSM-5 (412°C). The total acidity (μmol·g^{-1}) of the zeolites follow the order SSZ-13 (1277) > ZSM-5 (1062) > BEA (1008). The amounts of acid sites are close to the respective number of Al atoms, namely, SSZ-13 (1200), ZSM-5 (1050), and BEA (1247).

The results of surface area and acidity measurements of the Cu-, Fe-, and Mn-zeolite catalysts are summarized in Table 2. Surface area of the metal-zeolite catalysts are in the range and order of SSZ-13 (585–549) > BEA (528–518) > ZSM-5 (369–345). The change in the surface area from metal to metal on a given zeolite support is very small.

Figure 2(a) shows NH_3-TPD profiles of the fresh and hydrothermally treated Cu-zeolite catalysts in the temperature range 100–700°C. After impregnating Cu on zeolites, extra desorption peaks were observed between weak and moderate acid sites. These extra desorption peaks are resulting from the decomposition of a copper ammonia complex (NH_3 bonded to Cu cationic species) [27]. The total acidity of the Cu-zeolites is Cu-SSZ-13 (1792) > Cu-BEA (1759) > Cu-ZSM-5 (1671). The difference between the amounts of NH_3 desorbed from the Cu-zeolite and the corresponding zeolite is ascribed to the formation of complexes by interaction between ammonia molecules and copper cations $[Cu^{I}(NH_3)_x]^+$ ($x \geq 2$) [28]. The increase in acidity of the Cu-zeolite catalysts with the zeolite support is Cu-BEA (751) > Cu-ZSM-5 (609) > Cu-SSZ-13 (515), corresponding to molar NH_3/Cu ratios of Cu-BEA (1.59) > Cu-ZSM-5 (1.29) > Cu-SSZ-13 (1.09). The fact that these ratios are below 2 gives strong evidence for Cu not exclusively being present as isolated cationic species. The order of the number of added acid sites suggests that Cu-BEA is the catalyst with most copper cations located at the exchange sites of the zeolite, however, since x in $[Cu^{I}(NH_3)_x]^+$ is unknown, the differences are minor, and no clear conclusion can be drawn.

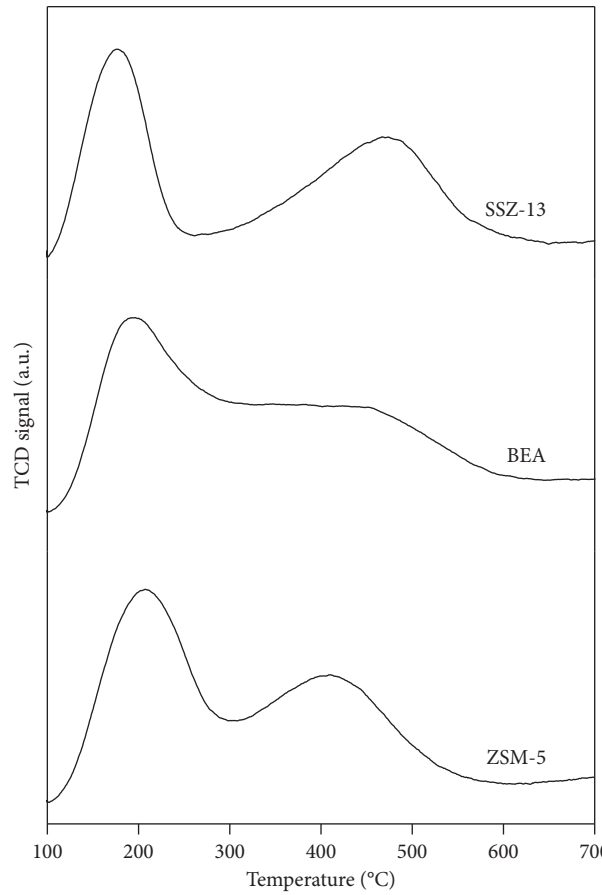

Figure 1: NH_3-TPD profiles of zeolite supports.

Hydrothermally treated Cu-zeolites showed a decrease in total acidity along with the shift of T_{max} of the NH_3 desorption peak to the lower region. Such a decrease in total acidity is probably due to dealumination of the zeolites but could also be due to migration of active, cationic copper species from the framework to form metal oxide particles [4, 8]. The extent of dealumination can be well monitored through ^{27}Al NMR analysis [8, 29]. Migration of copper active species can be monitored with H_2-TPR analysis and XPS surface composition, see the following discussion. The total acidity of the Cu-zeolites after hydrothermal treatment is in the order of Cu-SSZ-13-HT(1580) > Cu-ZSM-5-HT(1350) > Cu-BEA-HT(1186). The relative loss of acidity of the hydrothermally treated catalysts

Table 2: Physical characterization of catalysts.

Catalyst	Surface area ($m^2 \cdot g^{-1}$)	Total acidity (μmol of $NH_3 \cdot g^{-1}$)		Metal/Si ratio[a] (based on XPS)		Change (%)
		Fresh	HT	Fresh	HT	
Cu-SSZ-13	549	1792	1580	0.0280	0.0292	4
Cu-BEA	523	1759	1186	0.0187	0.0300	38
Cu-ZSM-5	345	1671	1350	0.0189	0.0253	25
Fe-SSZ-13	585	1338	1098	0.0454	0.0491	8
Fe-BEA	518	1772	1195	0.0219	0.0231	5
Fe-ZSM-5	369	1519	1018	0.0247	0.0276	11
Mn-SSZ-13	577	1611	1358	0.0335	0.0488	31
Mn-BEA	528	1419	956	0.0242	0.0263	8
Mn-ZSM-5	355	1436	1065	0.0251	0.0298	16

[a]Cu/Si bulk composition is 0.032, Fe/Si bulk composition is 0.036, and Mn/Si bulk composition is 0.037.

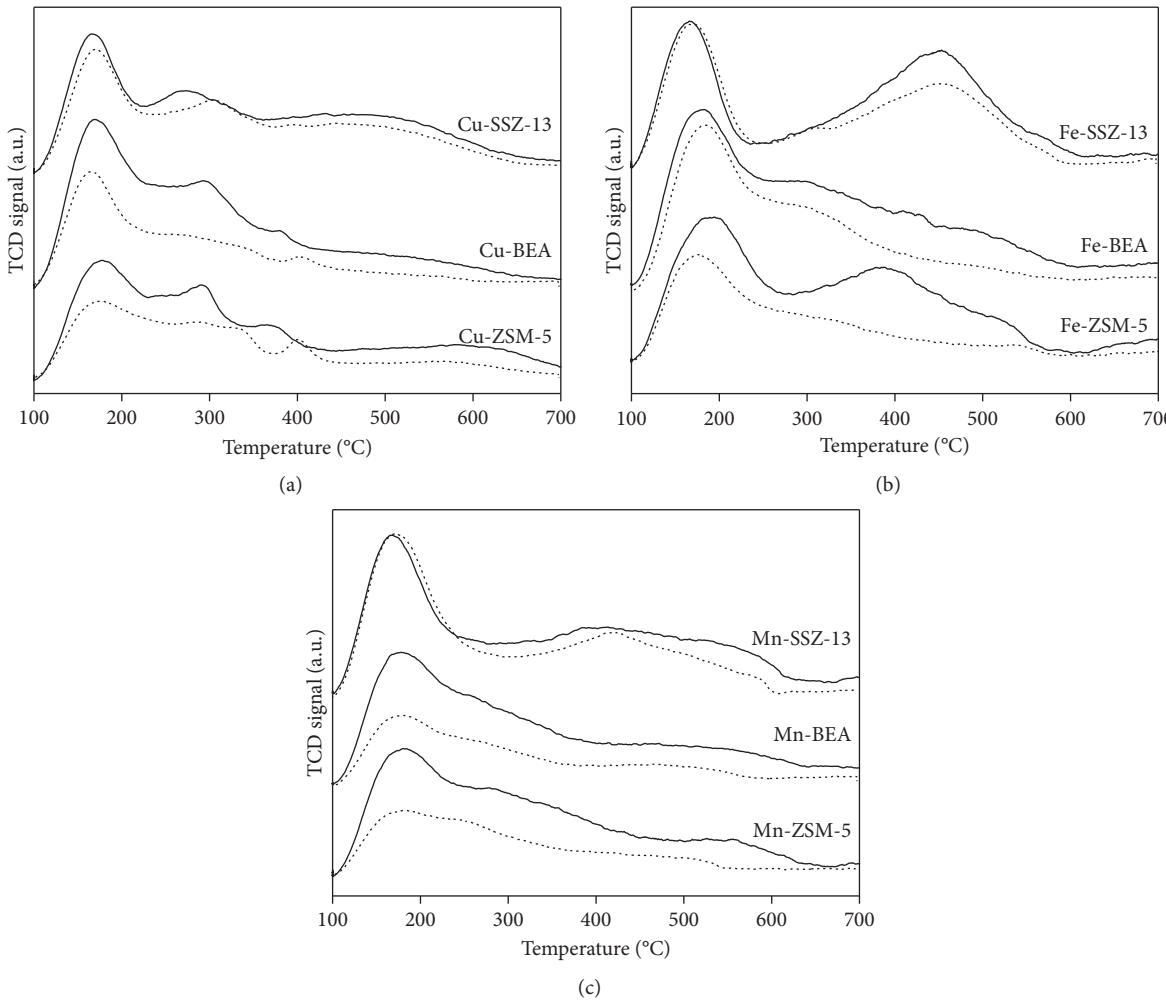

Figure 2: NH_3-TPD profiles of fresh and hydrothermally treated (dotted line) (a) Cu-, (b) Fe-, and (c) Mn-zeolite catalysts.

with respect to fresh Cu-zeolite catalysts is in the order Cu-BEA-HT (-573) > Cu-ZSM-5-HT (-321) > Cu-SSZ-13-HT (-212)>. The loss of acidity is also a function of pore size, as already known that small pore zeolites are more resistant to dealumination, whereby more retained acidity can be expected [29].

Figure 2(b) shows NH_3-TPD profiles of fresh and hydrothermally treated Fe-zeolite catalysts in the temperature range 100–700°C. All Fe-zeolites catalysts showed two ammonia desorption regions: one due to weak acid strength at the lower temperature and the other due to moderate acid strength at the high temperature. The total acidity of the Fe-

zeolites is Fe-BEA(1772) > Fe-ZSM-5(1519) > Fe-SSZ-13(1338). The increase in acidity of the Fe-zeolite catalysts with the zeolite support is Fe-BEA (764) > Fe-ZSM-5 (457) > Fe-SSZ-13 (61). Hydrothermally treated Fe-zeolite catalysts showed a less intense high temperature desorption peak along with loss in total acidity. The total acidity of the Fe-zeolites after hydrothermal treatment is Fe-BEA-HT(1195) > Fe-SSZ-13-HT(1098) > Fe-ZSM-5-HT(1018). The loss of acidity of the hydrothermally treated catalysts with respect to fresh Fe-zeolite catalysts is in the order Fe-BEA-HT (-577) > Fe-ZSM-5-HT (-501) > Fe-SSZ-13-HT (-240)>. As seen in Cu catalysts, the relative loss of acidity is a function of pore size with greater stability for small pores.

Figure 2(c) shows NH_3-TPD profiles of the fresh and hydrothermally treated Mn-zeolite catalysts in the temperature range 100–700°C. All Mn-zeolites catalysts showed two ammonia desorption regions: one due to weak acid strength at lower temperature and the other due to moderate acid strength at high temperature. The total acidity of the Mn-zeolites is Mn-SSZ-13(1611) > Mn-ZSM-5(1436) > Mn-BEA (1419). The difference between the amounts of NH_3 desorbed from the Mn-zeolite and the corresponding pure zeolite is Mn-BEA (411) > Mn-ZSM-5 (374) > Mn-SSZ-13 (334). Baran et al. [30] measured the number of acid sites of 2 wt.% Mn/Si-BEA prepared by impregnation. The authors used pyridine as the probe molecule at 150°C with FTIR detection and determined the number of Brønsted and Lewis acid sites to be 26 and 136 μmol/g, respectively. The corresponding number for SiBEA is 8 and 3 μmol/g. The increase of the number of Lewis acid sites was ascribed to the existence of framework mononuclear Mn species. The creation of Brønsted acid sites was explained by the presence of bridging hydroxyl groups in Si-O(H)-$Mn^{(III)}$. The difference between the number of acid sites due to Mn reported in the current study and by Baran et al. [30] can probably be explained by the differences in Mn loading (3 vs. 2 wt.%), characterization technique, and temperature range. The total acidity of the Mn-zeolites after hydrothermal treatment is Mn-SSZ-13-HT(1358) > Mn-ZSM-5-HT(1065) > Mn-BEA-5-HT(956). The loss of acidity of the hydrothermally treated catalysts with respect to fresh Mn-zeolite catalysts is in the order Mn-BEA-HT (-463) > Mn-ZSM-5 (-371)-HT > Mn-SSZ-13-HT (-253). Overall, all the catalysts exhibited increase in acidity after metal impregnation (Cu, Fe, and Mn), and after hydrothermal treatment, most of the catalysts lost significant amount of acidic sites.

3.1.3. H_2-TPR. H_2-TPR is frequently used to study the redox property of the catalysts. Fresh and hydrothermally treated Cu-zeolite catalysts TPR patterns are shown in Figure 3(a). The fresh Cu-zeolite catalysts showed peaks between 160 and 230°C. According to the literature, bulk copper oxide exhibits only one TPR peak attributed to direct reduction of Cu^{2+} ions to Cu^0 [31]. A large number of literature report on Cu-zeolites showing that Cu may belong to cations or nanosized polynuclear oxocations (n = 2, 3) located at exchange sites and supported CuO aggregates. The former are reduced into two steps: Cu^{2+} to Cu^+ at low temperature (<230°C) and then Cu^+ to Cu^0 at above 830°C. Cu-SSZ-13 and Cu-ZSM-5 catalysts showed a two-stage reduction with a shoulder peak that could be due to reduction of cationic Cu species at various exchange sites [29, 32]. Combined with the NH_3-TPD results, we conclude that Cu is probably both present in the form of cationic framework species as well as CuO_x particles. Figure 3(a) also shows the H_2-TPR patterns of hydrothermally treated Cu-zeolite catalysts (dotted line). Fresh and hydrothermally treated catalysts looked very similar except a slight shift of the reduction peaks to higher temperatures. Similar observations are also made on Cu-SAPO-34 and Cu-SSZ13 catalysts [8, 29]. Such a shift in reduction peaks to higher temperatures could be due to migration of copper from exchange sites to the surface or to strong interaction of Cu with the support [9, 29, 33]. This could indicate that the redox properties of the Cu-zeolite catalysts are altered by hydrothermal treatment.

The TPR profiles of Fe-zeolite catalysts are shown in Figure 3(b). The reduction of Fe species on the Fe-zeolites started at 200°C and continued till 850°C with profiles broadly divided into two regions: low temperature reduction region between 200 and 400°C and medium temperature reduction region between 400 and 700°C. According to the literature, the low temperature reduction peak can be attributed to the reduction of Fe^{3+} to Fe^{2+} species as well as the reduction of Fe_2O_3 to Fe_3O_4 [34, 35]. The medium temperature reduction peak corresponds to reduction of small nanoclusters of Fe_3O_4 to FeO and further reduction to Fe occurs at above 1000°C along with zeolite framework collapse [35, 36]. As evidenced in Figure 3(b), iron oxide reduction profiles are different for each catalyst. Hydrothermally treated catalysts showed a shift of the reduction patterns to higher temperatures. Such a change in the reduction temperature could be due to reduction of iron oxide clusters particles which have clustered during hydrothermal treatment [37].

The TPR profiles of Mn-zeolite catalysts are presented in Figure 3(c). The reduction of manganese oxide species is influenced by the MnO_x-support interaction. It can be seen that the reduction patterns are different for each support. The direct assignment of peaks is difficult. Three different reduction peaks are observed on all catalysts. These three different reduction peaks correspond to stepwise reduction of MnO_2 to MnO. The low temperature reduction peak below 250°C (MnO_2 to Mn_2O_3), medium temperature reduction peak around 300°C (Mn_2O_3 to Mn_3O_4), and a high temperature reduction peak between 350 and 450°C are observed (Mn_3O_4 to MnO) [38, 39]. Similar to Cu- and Fe-zeolites, hydrothermally treated Mn-zeolite catalysts also show a slight shift of reduction peaks to higher temperatures, which is regarded as an indication of strong interactions between oxide species and the support [39].

3.1.4. XPS. Surface composition (metal/Si ratio) of fresh and hydrothermally treated catalysts measured by XPS is summarized in Table 2. For all the fresh catalysts, except Fe-SSZ-

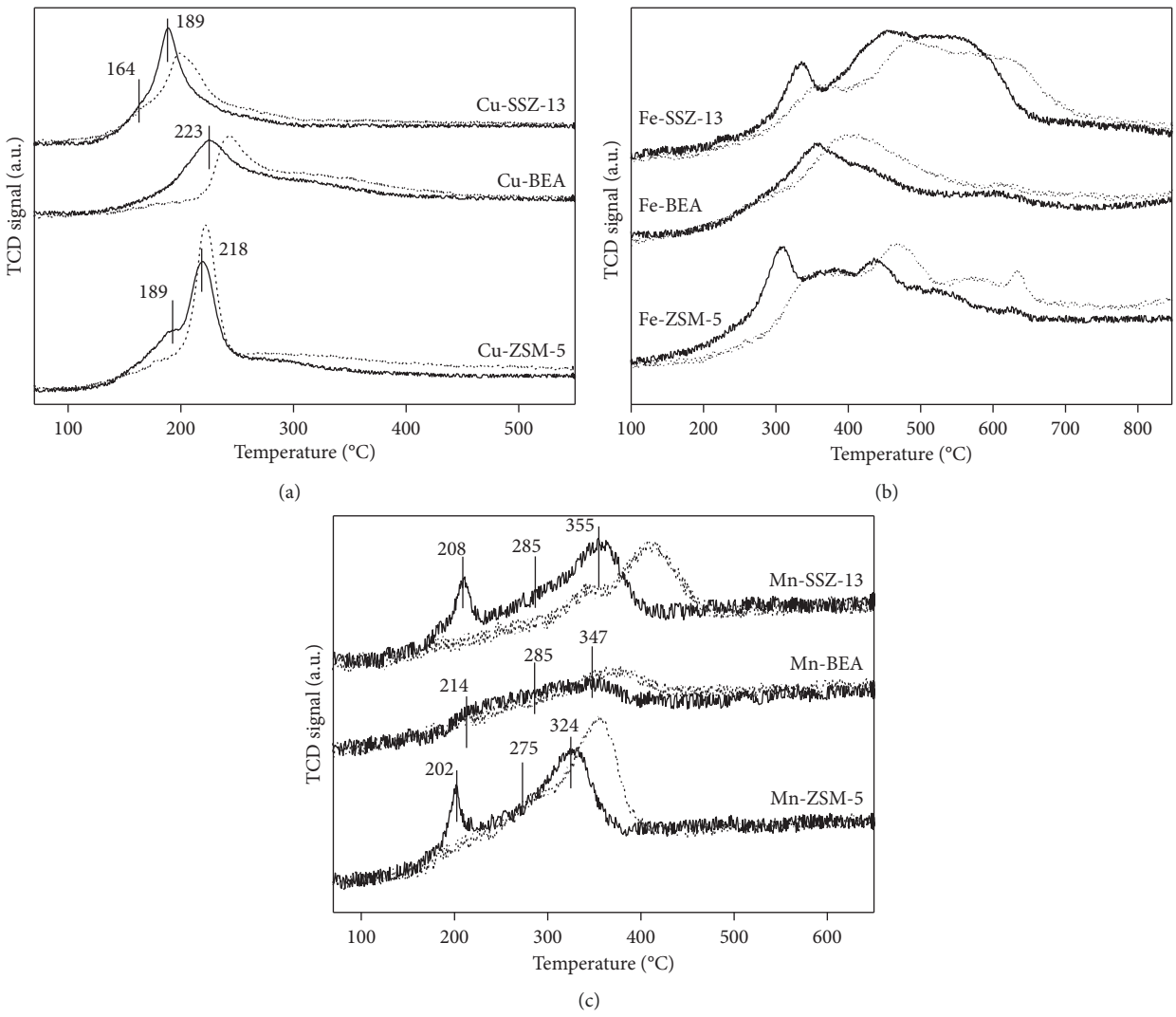

Figure 3: H_2-TPR profiles of fresh and hydrothermally treated (dotted line) (a) Cu-, (b) Fe-, and (c) Mn-zeolite catalysts.

13, the metal/Si ratios measured by XPS are lower than those corresponding to the bulk composition of the zeolites, indicating that the metal concentration in the surface of the zeolite is lower than those in the interior. The exceptional case of Fe-SSZ-13 could be due to Fe is not being incorporated in the zeolite due to the preparation method. Steric hindrance of highly solvated iron cations was reported to limit their diffusion into small pore zeolites [40, 41]. After hydrothermal treatment, the metal/Si ratio increased, suggesting that the metal migrated towards the external surface of the zeolite [42]. Overall, Fe-containing catalysts exhibit the smallest change with M/Si ratios increasing by only 5 to 11%. Manganese-containing catalysts show increases between 9 and 45%, while the copper-containing catalysts are the most affected ones with M/Si ratio increase between 4 and 60%. These values suggest that the iron species are less affected by hydrothermal treatment at 650°C and less prone to migration to the outer surface than the manganese and copper species are. Notably, there is a minor increase of the metal/Si ratio in the Cu-SSZ-13, Fe-BEA, and Mn-BEA catalysts.

3.2. NH_3-SCR Activity Results

3.2.1. Cu-Zeolites. The catalytic activity of the fresh and hydrothermal treated Cu-zeolite catalysts was measured in the temperature range 250–550°C. In Figure 4, the catalytic activities obtained are shown as the first-order mass-based rate constant ($cm^3 \cdot g^{-1} \cdot s^{-1}$). All the catalysts showed increase in activity with increase in reaction temperature, reaching a maximum value and decreases thereafter due to the increased rate of ammonia oxidation. Cu-SSZ-13, Cu-BEA, and Cu-ZSM-5 catalysts showed maximum rate constants of 1443, 1688 ,and 1753 $cm^3 \cdot g^{-1} \cdot s^{-1}$ at their T_{max} of 450, 550, and 425°C, respectively. The difference in T_{max} exhibited during the SCR of NO could be due to a change in ease of reduction of copper oxide and ammonia adsorption strength [32]. Irrespective of the T_{max}, all the Cu-zeolites catalysts showed high SCR activity in the temperature window of 350–550°C. The Cu-SSZ-13 catalyst exhibits a different activity profile with two maximum rate constants of 832 and 1443 $cm^3 \cdot g^{-1} \cdot s^{-1}$ at low (325°C) and high reaction temperatures (450°C), respectively. The fact that the activity profile of Cu-SSZ-13 posses one global (at 450°C)

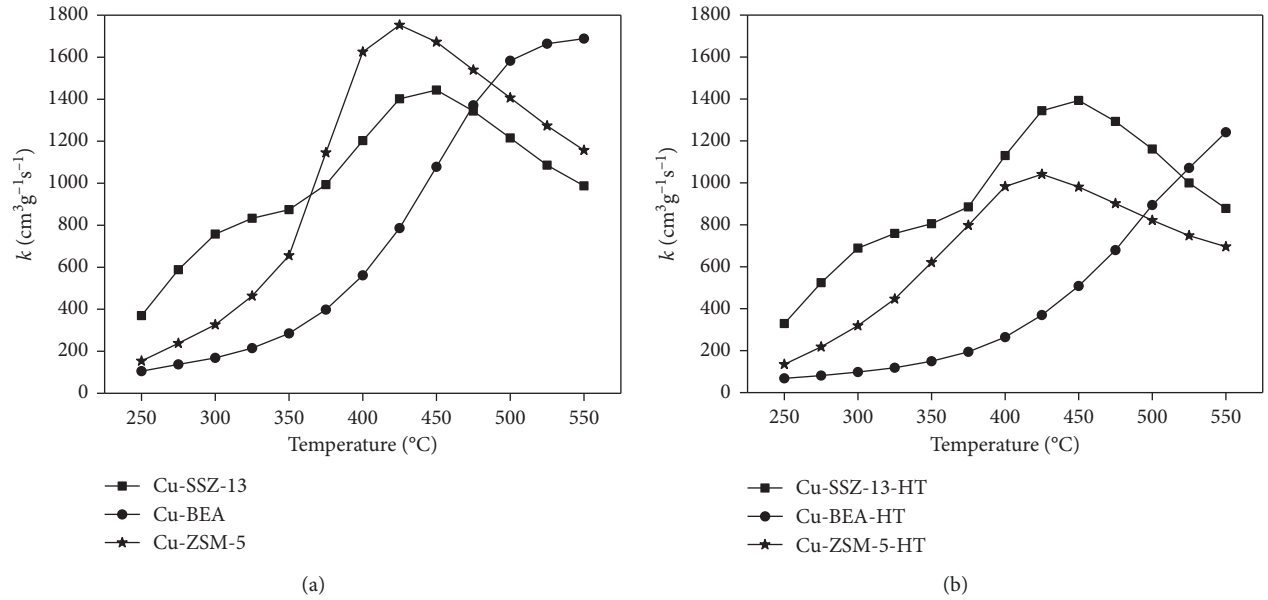

Figure 4: SCR activity of (a) fresh and (b) hydrothermally treated Cu-zeolites.

and one local maximum (at 325°C) could be due to location of Cu active sites in two different sites of SSZ-13 as also observed by Kwak et al. [29, 43].

Hydrothermally treated Cu-zeolite SCR activity profiles are shown in Figure 4. All the catalysts showed similar activity profile patterns as the fresh catalysts. Cu-SSZ-13-HT, Cu-BEA-HT, and Cu-ZSM-5-HT catalysts exhibit maximum rate constants of 1393, 1241, and 1041 $cm^3 \cdot g^{-1} \cdot s^{-1}$ at their T_{max} of 450, 550, and 425°C, respectively. Except for the Cu-SSZ-13, the catalysts lost significant SCR activity. The superior hydrothermal resistance of the small-pore Cu-SSZ-13 catalyst is better than medium and large pore zeolites [6, 7]. In the present investigation, along with the small-pore size effect, the superior hydrothermal stability of Cu-SSZ-13 may also be related to the retained total acidity and the similar redox pattern.

3.2.2. Fe-Zeolites. The catalytic activity of the fresh and the hydrothermally treated Fe-zeolite catalysts is shown in Figure 5. All the catalysts showed increase in activity with an increase in reaction temperature. Fe-zeolite catalysts are known to be performing well at high temperatures, e.g., in a temperature window of 400–600°C [37, 44]. Fe-SSZ-13, Fe-BEA, and Fe-ZSM-5 catalysts exhibit maximum rate constants of 102, 593, and 544 $cm^3 \cdot g^{-1} \cdot s^{-1}$, respectively, at their T_{max} of 525°C. Fe-CHA (chabazite zeolite) catalysts activity was reported to be lower than Fe-MOR and Fe-BEA catalysts [45]. Compared to the Cu-zeolites, the SCR activity of the Fe-zeolites is lower and T_{max} temperatures are higher. Especially, Fe-SSZ-13 exhibits much lower activity. Very poor activity of Fe-SSZ-13 shows that impregnation might not be the best method to incorporate Fe. Instead other catalyst preparation techniques like conventional ion exchange and chemical vapour ion exchange are recommended [4]. Hydrothermally treated Fe-zeolite SCR activity profiles are shown in Figure 5. Fe-SSZ-13-HT, Fe-BEA-HT, and Fe-ZSM-5-HT catalysts exhibit maximum rate constants of 57, 610, and 474 $cm^3 \cdot g^{-1} \cdot s^{-1}$ at their T_{max} of 550, 550, and 525°C, respectively. Except for Fe-BEA, Fe-zeolite catalysts lost significant SCR activity. The hydrothermal resistance of Fe-BEA catalyst has earlier been reported [4, 46–48].

According to Balle et al. [48], the superior hydrothermal resistance of the Fe-BEA catalyst is due to the retained structure of the Fe sites, the slight decrease in surface area, and total acidity. The Fe-zeolite catalysts do not exhibit the small-pore size effect or the retained total acidity pattern to correlate the activity. Moderate hydrothermal resistance of Fe-BEA catalyst could be due to retained redox patterns under this milder hydrothermal condition. According to Shwan et al. [49], hydrothermal treatment is classified as milder and severe aging processes. Milder aging transforms isolated iron species to oligomeric iron clusters in the zeolite pores and further aging results in migration and formation of large iron oxide particles on the external surface of the zeolite. Oligomeric iron cluster formation inside the pores should not alter the surface Fe/Si ratio as measured by XPS. Migration of iron from the pores to the surface followed by the formation of large iron oxide particles does not necessarily increase the Fe/Si ratio as measured by XPS. This is because the FeO_x particle might become bigger than the penetration depth of the X-rays of a few nanometers. The fact that the surface Fe/Si ratios did not change might either be a sign of no iron migrating to the surface as is expected under mild hydrothermal treatment or that a possible migration to the surface is accompanied by formation of clusters too big to be fully recorded by XPS.

3.2.3. Mn-Zeolites. The catalytic activity of the fresh and hydrothermally treated Mn-zeolite catalysts is shown in Figure 6. The Mn-SSZ-13, Mn-BEA, and Mn-ZSM-5 catalysts exhibit maximum rate constants of 386, 153, and

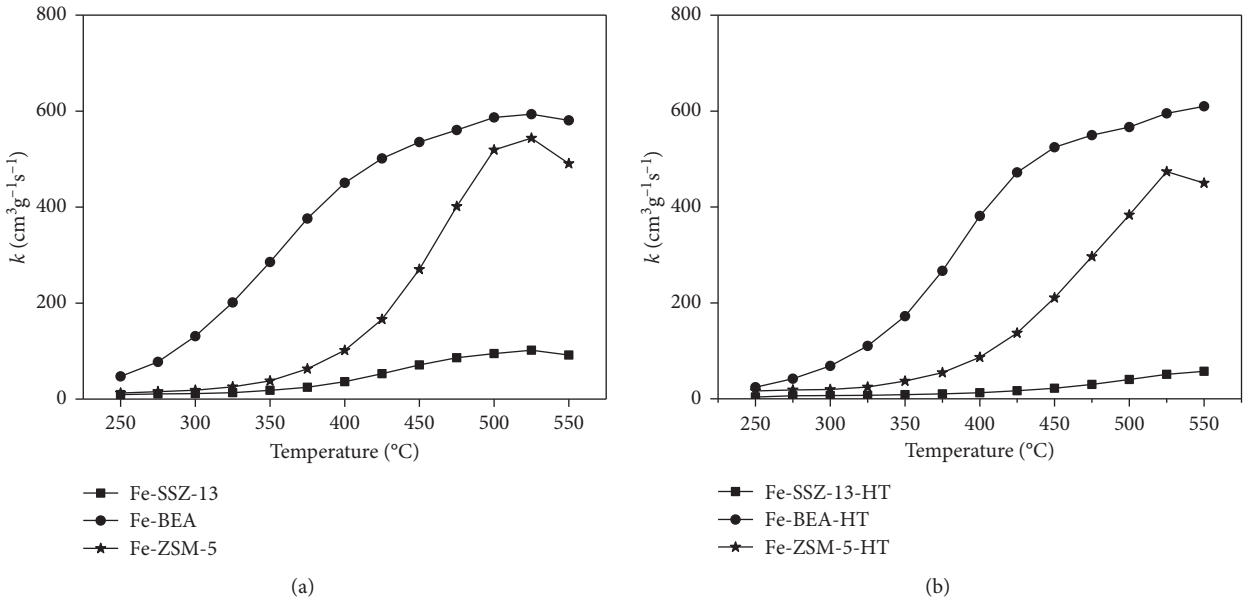

Figure 5: SCR activity of (a) fresh and (b) hydrothermally treated Fe-zeolites.

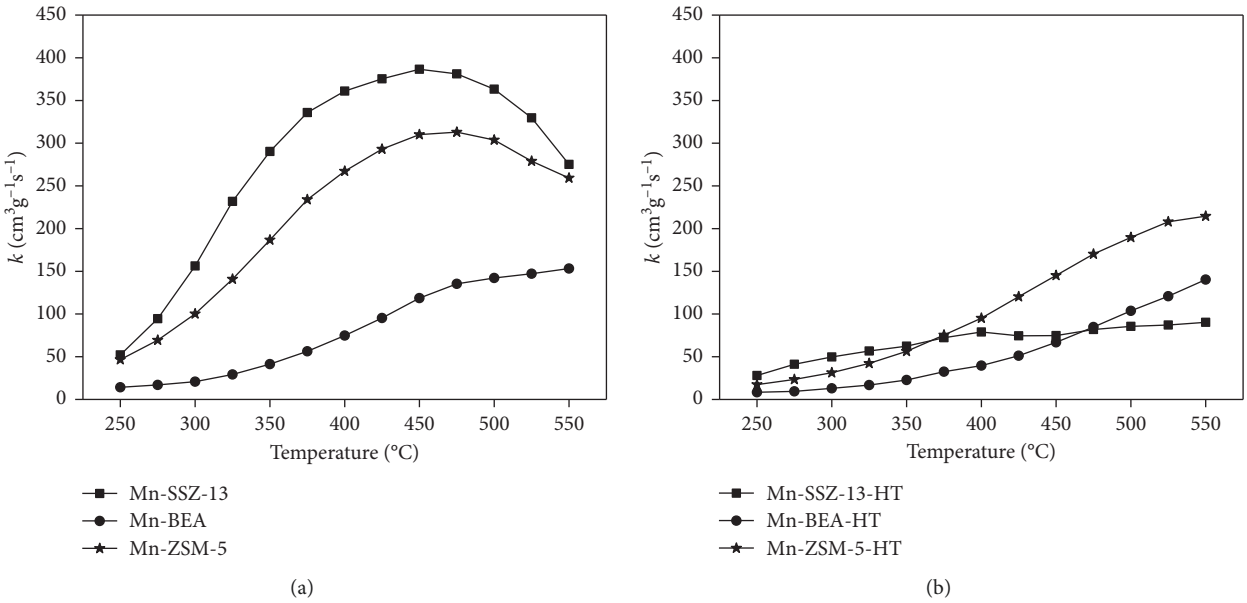

Figure 6: SCR activity of (a) fresh and (b) hydrothermally treated Mn-zeolites.

313 cm^3·g^{-1}·s^{-1} at their T_{max} of 450, 550, and 475°C, respectively. Compared to Cu-zeolites and Fe-zeolites, the SCR activity of Mn-zeolites is lower. Mn-SSZ-13-HT, Mn-BEA-HT, and Mn-ZSM-5-HT catalysts exhibit maximum rate constants of 90, 140, and 215 cm^3·g^{-1}·s^{-1} at their T_{max} of 550°C, respectively. All Mn-zeolite catalysts lost significant SCR activity by the hydrothermal treatment. SCR activities of the present catalysts (Cu, Fe, and Mn) are not compared with the open literature because each metal and support might have its own optimum regarding loading and choice of the preparation method.

3.3. Resistance to Hydrothermal Treatment. The relative retained catalytic activity at 300, 400, and 500°C of Cu-, Fe-, and Mn-zeolites after hydrothermal treatment is shown in Figure 7. Cu-zeolite catalysts exhibit a relative activity in the order Cu-SSZ-13 > Cu-ZSM-5 > Cu-BEA at all three temperatures. The relative activity of the Cu-zeolite catalysts can be correlated with small-pore size, retained total acidity, and less migration of Cu species. At 500°C, Fe-zeolite catalysts follow the order of Fe-BEA > Fe-ZSM-5 > Fe-SSZ-13. At 400°C, the order is very similar, being Fe-BEA = Fe-ZSM-5 > Fe-SSZ-13, and at 300°C, only Fe-BEA exhibits and retains a

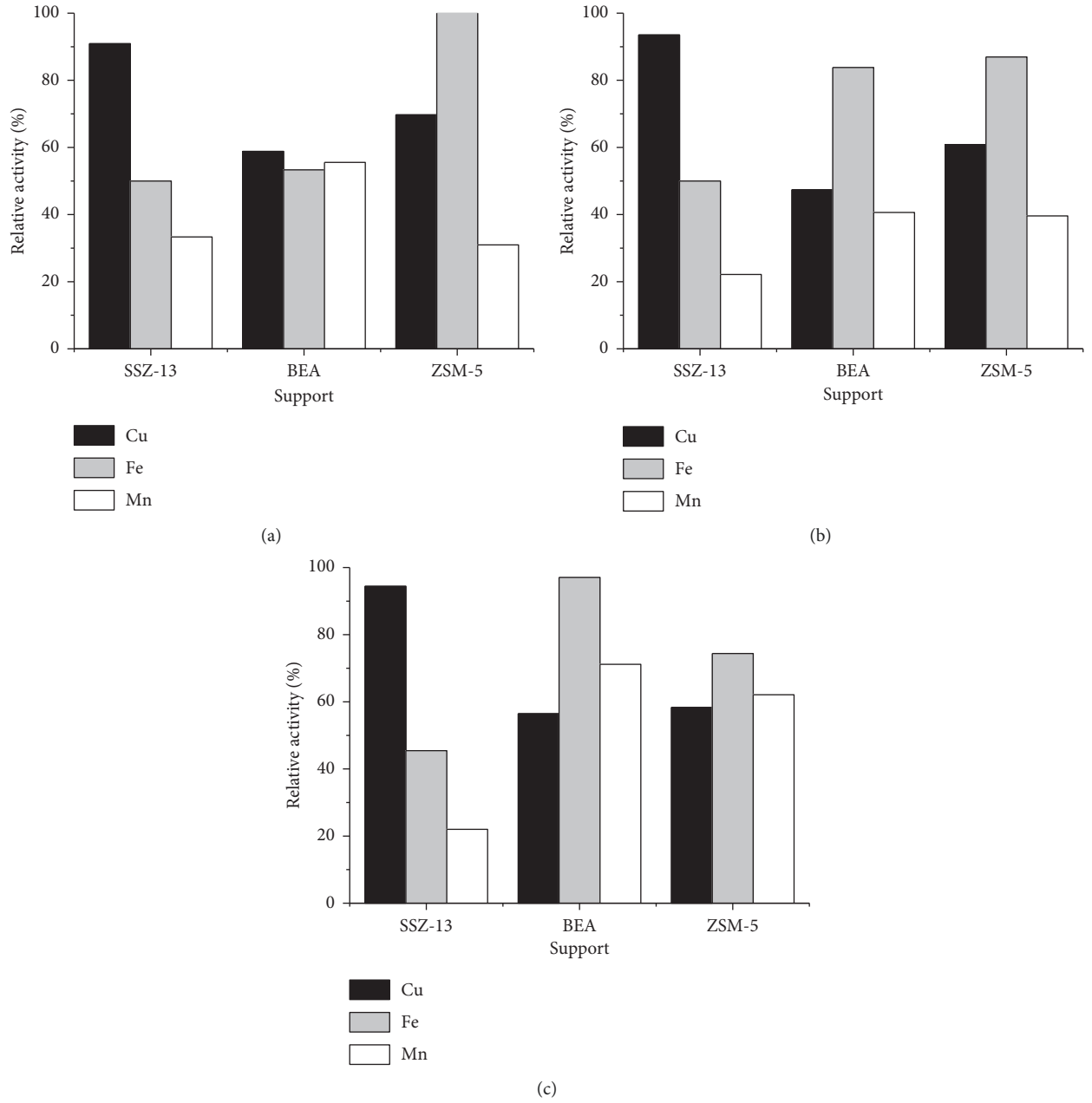

Figure 7: Relative catalytic activity (%) of Cu-zeolite, Fe-zeolite, and Mn-zeolite at (a) 300, (b) 400, and (c) 500°C.

relatively high degree of activity. Out of the manganese-containing catalysts, Mn-BEA is the most resistant one at all three temperatures, however, starting from a very low fresh activity. Its high resistance to hydrothermal treatment coincides with its H_2-TPR profile being the least affected one but is in contradiction to it showing the highest loss in acid sites. At 400 and 500°C, Mn-SSZ-13 which is the most active catalyst in the fresh state retains only about 20 % of its activity, while Mn-ZSM-5 retains about 40 and 62%. Fe and Mn-zeolite catalysts do not follow the small-pore size effect and the trend of retained total acidity. Among all investigated catalysts, the Cu-SSZ-13 and Fe-BEA exhibit the most promising stabilities and activities after hydrothermal treatment.

3.4. N_2O Formation. The catalytic selectivity in terms of N_2O formation was observed at 450°C. Cu-SSZ-13, Cu-ZSM-5, and Cu-BEA catalysts displayed N_2O concentration of 8 ppm, 15 ppm, and 25 ppm, respectively. Fe-SSZ-13, Fe-ZSM-5, and Fe-BEA catalysts did not display N_2O formation. Mn-SSZ-13, Mn-ZSM-5, and Mn-BEA catalysts displayed N_2O concentration of 12 ppm, 26 ppm, and 38 ppm, respectively. The highly active and hydrothermally resistant Cu-SSZ-13 catalyst performs also well regarding the level of N_2O formation.

4. Conclusions

Cu-, Fe-, and Mn-zeolite catalysts are active for the SCR of NO with NH_3. Increased total acidity after metal

impregnation and loss of acidity due to hydrothermal treatment are observed. Cu-zeolites and Mn-zeolites showed medium temperature catalytic activity, and Fe-zeolites showed high temperature activity. The resistance against hydrothermal treatment is dependent on the type of metal and support. Among all the catalysts, Cu-SSZ-13 and Fe-BEA catalysts are the most promising hydrothermal-resistant catalysts. Hydrothermal resistance of Cu-SSZ-13 catalyst is a function of small pore size and retained acidic and redox properties, which in term can be seen with respect to minor increase in migration of Cu species to the surface of the zeolite. Fe- and Mn-zeolite catalysts do not follow the small-pore size or retained acidic redox properties effect.

Data Availability

All the data present were generated in house or are properly referenced.

Conflicts of Interest

The authors declare that they have no conflicts of interest.

Acknowledgments

This work has been financially supported by Energinet.dk through the PSO projects 2009-1-10521 and 2013-1-12096.

References

[1] E. T. C. Vogt, A. J. V. Dillen, J. W. Geus, and F. J. J. G. Janssen, "Selective catalytic reduction of NO_x with NH_3 over a V_2O_5/TiO_2 on silica catalyst," *Catalysis Today*, vol. 2, no. 5, pp. 569–579, 1988.

[2] M. Shigeru, Y. Hideto, T. Kazumasa, and K. Satoru, "Improvement of V_2O_5-TiO_2 catalyst for No_x reduction with NH_3 in flue gases," *Chemistry Letters*, vol. 10, no. 2, pp. 251–254, 1981.

[3] G. Busca, L. Lietti, G. Ramis, and F. Berti, "Chemical and mechanistic aspects of the selective catalytic reduction of NO_x by ammonia over oxide catalysts : a review," *Applied Catalysis B: Environmental*, vol. 18, no. 1-2, pp. 1–36, 1998.

[4] S. Brandenberger, O. Kröcher, A. Tissler, and R. Althoff, "The state of the art in selective catalytic reduction of NO_x by ammonia using metal-exchanged zeolite catalysts," *Catalysis Reviews*, vol. 50, no. 4, pp. 492–531, 2008, ISBN 0161-4940r1520-5703.

[5] T. Seiyama, "Catalytic activity of transition metal ion exchanged Y zeolites in the reduction of nitric oxide with ammonia," *Journal of Catalysis*, vol. 48, no. 1–3, pp. 1–7, 1977.

[6] J. H. Kwak, R. G. Tonkyn, D. H. Kim, J. Szanyi, and C. H. F. Peden, "Excellent activity and selectivity of Cu-SSZ-13 in the selective catalytic reduction of NO_x with NH_3," *Journal of Catalysis*, vol. 275, no. 2, pp. 187–190, 2010.

[7] D. W. Fickel, E. D'Addio, J. A. Lauterbach, and R. F. Lobo, "The ammonia selective catalytic reduction activity of copper-exchanged small-pore zeolites," *Applied Catalysis B: Environmental*, vol. 102, no. 3-4, pp. 441–448, 2011.

[8] L. Ma, Y. Cheng, G. Cavataio, R. W. McCabe, L. Fu, and J. Li, "Characterization of commercial Cu-SSZ-13 and Cu-SAPO-34 catalysts with hydrothermal treatment for NH_3-SCR of NO_x in diesel exhaust," *Chemical Engineering Journal*, vol. 225, pp. 323–330, 2013.

[9] J. S. McEwen, T. Anggara, W. F. Schneider et al., "Integrated operando X-ray absorption and DFT characterization of Cu-SSZ-13 exchange sites during the selective catalytic reduction of NO_x with NH_3," *Catalysis Today*, vol. 184, no. 1, pp. 129–144, 2012.

[10] C. Paolucci, I. Khurana, A. A. Parekh et al., "SI-Dynamic multinuclear sites formed by mobilized copper ions in NO_x selective catalytic reduction," *Science*, vol. 357, no. 6354, pp. 898–903, 2017.

[11] Y. Xin, Q. Li, and Z. Zhang, "Zeolitic materials for $DeNO_x$ selective catalytic reduction," *ChemCatChem*, vol. 10, no. 1, pp. 29–41, 2017.

[12] K. A. Lomachenko, E. Borfecchia, C. Negri et al., "The Cu-CHA $deNO_x$ catalyst in action: temperature-dependent NH_3-assisted selective catalytic reduction monitored by operando XAS and XES," *Journal of the American Chemical Society*, vol. 138, no. 37, pp. 12025–12028, 2016.

[13] H. Falsig, P. N. R. Vennestrøm, P. G. Moses, and T. V. W. Janssens, "Activation of oxygen and NO in NH_3-SCR over Cu-CHA catalysts evaluated by density functional theory," *Topics in Catalysis*, vol. 59, no. 10–12, pp. 861–865, 2016.

[14] T. V. W. Janssens, H. Falsig, L. F. Lundegaard et al., "A consistent reaction scheme for the selective catalytic reduction of nitrogen oxides with ammonia," *ACS Catalysis*, vol. 5, no. 5, pp. 2832–2845, 2015.

[15] J. Wang, D. Fan, T. Yu et al., "Improvement of low-temperature hydrothermal stability of Cu/SAPO-34 catalysts by Cu^{2+} species," *Journal of Catalysis*, vol. 322, pp. 84–90, 2015.

[16] C. Niu, X. Shi, K. Liu, Y. You, S. Wang, and H. He, "A novel one-pot synthesized CuCe-SAPO-34 catalyst with high NH_3-SCR activity and H_2O resistance," *Catalysis Communications*, vol. 81, pp. 20–23, 2016.

[17] E. Y. Choi, I. S. Nam, and Y. G. Kim, "TPD study of mordenite-type zeolites for selective catalytic reduction of NO by NH_3," *Journal of Catalysis*, vol. 161, no. 2, pp. 597–604, 1996.

[18] M. Mizumoto, N. Yamazoe, and T. Seiyama, "Catalytic reduction of NO with ammonia over Cu(II) NaY," *Journal of Catalysis*, vol. 55, no. 2, pp. 119–128, 1978.

[19] C. Paolucci, A. A. Verma, S. A. Bates et al., "Isolation of the copper redox steps in the standard selective catalytic reduction on Cu-SSZ-13," *Angewandte Chemie–International Edition*, vol. 53, no. 44, pp. 11828–11833, 2014.

[20] M. Richter, A. Trunschke, U. Bentrup et al., "Selective catalytic reduction of nitric oxide by ammonia over egg-shell MnO_x/NaY composite catalysts," *Journal of Catalysis*, vol. 206, no. 1, pp. 98–113, 2002.

[21] F. Gao, E. D. Walter, M. Kollar, Y. Wang, J. Szanyi, and C. H. F. Peden, "Understanding ammonia selective catalytic reduction kinetics over Cu/SSZ-13 from motion of the Cu ions," *Journal of Catalysis*, vol. 319, pp. 1–14, 2014.

[22] F. Giordanino, P. N. R. Vennestrøm, L. F. Lundegaard et al., "Characterization of Cu-exchanged SSZ-13: a comparative FTIR, UV-Vis, and EPR study with Cu-ZSM-5 and Cu-β with similar Si/Al and Cu/Al ratios," *Dalton Transactions*, vol. 42, no. 35, pp. 12741–12761, 2013.

[23] N. Wilken, R. Nedyalkova, K. Kamasamudram et al., "Investigation of the effect of accelerated hydrothermal aging on the Cu sites in a Cu-BEA catalyst for NH_3-SCR applications," *Topics in Catalysis*, vol. 56, no. 1–8, pp. 317–322, 2013.

[24] R. Q. Long and R. T. Yang, "Catalytic performance and characterization of VO2+-exchanged titania-pillared clays for selective catalytic reduction of nitric oxide with ammonia," *Journal of Catalysis*, vol. 196, no. 1, pp. 73–85, 2000.

[25] S. S. R. Putluru, A. D. Jensen, A. Riisager, and R. Fehrmann, "Heteropoly acid promoted V_2O_5/TiO_2 catalysts for NO abatement with ammonia in alkali containing flue gases," *Catalysis Science and Technology*, vol. 1, no. 4, p. 631, 2011.

[26] S. A. Bates, W. N. Delgass, F. H. Ribeiro, J. T. Miller, and R. Gounder, "Methods for NH_3 titration of Brønsted acid sites in Cu-zeolites that catalyze the selective catalytic reduction of NO_x with NH_3," *Journal of Catalysis*, vol. 312, pp. 26–36, 2014.

[27] A. V. Salker and W. Weisweiler, "Catalytic behaviour of metal based ZSM-5 catalysts for NO_x reduction with NH_3 in dry and humid conditions," *Applied Catalysis A: General*, vol. 203, no. 2, pp. 221–229, 2000.

[28] S. Shwan, M. Skoglundh, L. F. Lundegaard et al., "Solid-state ion-exchange of copper into zeolites facilitated by ammonia at low temperature," *ACS Catalysis*, vol. 5, no. 1, pp. 16–19, 2015.

[29] J. H. Kwak, D. Tran, S. D. Burton, J. Szanyi, J. H. Lee, and C. H. F. Peden, "Effects of hydrothermal aging on NH_3-SCR reaction over Cu/zeolites," *Journal of Catalysis*, vol. 287, pp. 203–209, 2012.

[30] R. Baran, L. Valentin, J. M. Krafft, T. Grzybek, P. Glatzel, and S. Dzwigaj, "Influence of the nature and environment of manganese in Mn-BEA zeolites on NO conversion in selective catalytic reduction with ammonia," *Physical Chemistry Chemical Physics*, vol. 19, no. 21, pp. 13553–13561, 2017.

[31] Á. Szegedi, Z. Kónya, D. Méhn et al., "Spherical mesoporous MCM-41 materials containing transition metals: synthesis and characterization," *Applied Catalysis A: General*, vol. 272, no. 1-2, pp. 257–266, 2004.

[32] S. S. R. Putluru, A. Riisager, and R. Fehrmann, "Alkali resistant Cu/zeolite deNO_x catalysts for flue gas cleaning in biomass fired applications," *Applied Catalysis B: Environmental*, vol. 101, no. 3-4, pp. 183–188, 2011.

[33] O. Bortnovsky, P. Sazama, and B. Wichterlova, "Cracking of pentenes to C2–C4 light olefins over zeolites and zeotypes: role of topology and acid site strength and concentration," *Applied Catalysis A: General*, vol. 287, no. 2, pp. 203–213, 2005.

[34] R. Q. Long and R. T. Yang, "Selective catalytic reduction of NO with ammonia over FE3+-exchanged mordenite (FE-MOR): catalytic performance, characterization, and mechanistic study," *Journal of Catalysis*, vol. 207, no. 2, pp. 274–285, 2002.

[35] H. Lee and H. Rhee, "Stability of Fe/ZSM-5 de-NO_x catalyst : effects of iron loading and remaining Brønsted acid sites," *Catalysis Letters*, vol. 61, no. 1-2, pp. 71–76, 1999.

[36] A. Guzman-vargas, G. Delahay, and B. Coq, "Catalytic decomposition of N_2O and catalytic reduction of N_2O and N_2O + NO by NH_3 in the presence of O_2 over Fe-zeolite," *Applied Catalysis B: Environmental*, vol. 42, pp. 369–379, 2003.

[37] S. Brandenberger, O. Kröcher, M. Casapu, A. Tissler, and R. Althoff, "Hydrothermal deactivation of Fe-ZSM-5 catalysts for the selective catalytic reduction of NO with NH_3," *Applied Catalysis B: Environmental*, vol. 101, no. 3-4, pp. 649–659, 2011.

[38] A. Sultana, M. Sasaki, and H. Hamada, "Influence of support on the activity of Mn supported catalysts for SCR of NO with ammonia," *Catalysis Today*, vol. 185, no. 1, pp. 284–289, 2012.

[39] A. Derylo-Marczewska, W. Gac, N. Popivnyak, G. Zukocinski, and S. Pasieczna, "The influence of preparation method on the structure and redox properties of mesoporous Mn-MCM-41 materials," *Catalysis Today*, vol. 114, no. 2-3, pp. 293–306, 2006.

[40] I. Melián-Cabrera, S. Espinosa, J. C. Groen, B. V. D. Linden, F. Kapteijn, and J. A. Moulijn, "Utilizing full-exchange capacity of zeolites by alkaline leaching: preparation of Fe-ZSM5 and application in N_2O decomposition," *Journal of Catalysis*, vol. 238, no. 2, pp. 250–259, 2006.

[41] A. Shishkin, H. Kannisto, P. A. Carlsson, H. Härelind, and M. Skoglundh, "Synthesis and functionalization of SSZ-13 as an NH_3-SCR catalyst," *Catalysis Science and Technology*, vol. 4, no. 11, pp. 3917–3926, 2014.

[42] P. Budi, E. Curry-hyde, and R. F. Howe, "Stabilization of CuZSM-5 NO_x reduction catalysts with lanthanum," *Catalysis Letters*, vol. 41, no. 1-2, pp. 47–53, 1996.

[43] J. Hun Kwak, H. Zhu, J. H. Lee, C. H. F. Peden, and J. Szanyi, "Two different cationic positions in Cu-SSZ-13?," *Chemical Communications*, vol. 48, no. 39, pp. 4758–4760, 2012.

[44] S. S. R. Putluru, A. D. Jensen, A. Riisager, and R. Fehrmann, "Alkali resistant Fe-zeolite catalysts for SCR of NO with NH_3 in flue gases," *Topics in Catalysis*, vol. 54, no. 16–18, pp. 1286–1292, 2011.

[45] R. Q. Long and R. T. Yang, "Reaction mechanism of selective catalytic reduction of NO with NH_3 over Fe-ZSM-5 catalyst," *Journal of Catalysis*, vol. 207, no. 2, pp. 224–231, 2002.

[46] C. He, Y. Wang, Y. Cheng, C. K. Lambert, and R. T. Yang, "Activity, stability and hydrocarbon deactivation of Fe/Beta catalyst for SCR of NO with ammonia," *Applied Catalysis A: General*, vol. 368, no. 1-2, pp. 121–126, 2009.

[47] J. A. Z. Pieterse, G. D. Pirngruber, J. A. van Bokhoven, and S. Booneveld, "Hydrothermal stability of Fe-ZSM-5 and Fe-BEA prepared by wet ion-exchange for N_2O decomposition," *Studies in Surface Science and Catalysis*, vol. 170, pp. 1386–1391, 2007.

[48] P. Balle, B. Geiger, D. Klukowski et al., "Study of the selective catalytic reduction of NO_x on an efficient Fe/HBEA zeolite catalyst for heavy duty diesel engines," *Applied Catalysis B: Environmental*, vol. 91, no. 3-4, pp. 587–595, 2009.

[49] S. Shwan, E. C. Adams, J. Jansson, and M. Skoglundh, "Effect of thermal ageing on the nature of iron species in Fe-BEA," *Catalysis Letters*, vol. 143, no. 1, pp. 43–48, 2013.